HHS Public Access

Author manuscript

Mol Psychiatry. Author manuscript; available in PMC 2019 April 26.

Published in final edited form as:

Mol Psychiatry. 2019 May ; 24(5): 710–725. doi:10.1038/s41380-018-0245-8.

Genetic identification of a population of noradrenergic neurons implicated in attenuation of stress-related responses

Yu-Wei Chen, Ph.D.[1], **Manasmita Das, Ph.D.**[2], **Esteban A. Oyarzabal, B.S.**[2], **Qing Cheng, Ph.D.**[1], **Nicholas W. Plummer, Ph.D.**[1], **Kathleen G. Smith, B.S.**[1], **Grace K. Jones, B.S.**[1], **Daniel Malawsky**[1], **Jerrel L. Yakel, Ph.D.**[1], **Yen-Yu Ian Shih, Ph.D.**[2], and **Patricia Jensen, Ph.D.**[1]

[1]Neurobiology Laboratory, National Institute of Environmental Health Sciences, National Institutes of Health, Department of Health and Human Services, Research Triangle Park, NC, USA.

[2]Department of Neurology, University of North Carolina, Chapel Hill, NC, USA.

Abstract

Noradrenergic signaling plays a well-established role in promoting the stress response. Here we identify a subpopulation of noradrenergic neurons, defined by developmental expression of *Hoxb1*, that has a unique role in modulating stress-related behavior. Using an intersectional chemogenetic strategy, in combination with behavioral and physiological analyses, we show that activation of *Hoxb1*-noradrenergic (*Hoxb1*-NE) neurons decreases anxiety-like behavior and promotes an active coping strategy in response to acute stressors. In addition, we use cerebral blood volume (CBV)-weighted functional magnetic resonance imaging to show that chemoactivation of *Hoxb1*-NE neurons results in reduced activity in stress-related brain regions, including the bed nucleus of the stria terminalis (BNST), amygdala, and locus coeruleus. Thus, the actions of *Hoxb1*-NE neurons are distinct from the well documented functions of the locus coeruleus in promoting the stress response, demonstrating that the noradrenergic system contains multiple functionally distinct subpopulations.

Correspondence to: Patricia Jensen, Ph.D., Neurobiology Laboratory, National Institute of Environmental Health Sciences, 111 T.W. Alexander Drive, Bldg. 101, Rm. F118 (Mail Drop F1-11), Research Triangle Park, NC 27709, Tel.: 919-541-0379, patricia.jensen@nih.gov.

Author Contributions

Y.W.C. and P.J. conceived, designed, and supervised the project. The behavioral and physiological tests were performed by Y.W.C. and G.J., and analyzed by Y.W.C. The fMRI experiments and analyses were performed by M.D. and E.A.O. under the guidance of Y.Y.I.S.; Q.C. performed the electrophysiological recordings under the guidance of J.L.Y.; Immunohistochemistry, *in situ* hybridization, and image acquisition was performed by K.G.S, G.J., D.M. and N.W.P.; Cell counts were performed by D.M. and G.J.; Y.W.C. and P.J. wrote the manuscript with input from co-authors.

Conflict of Interest

The authors declare no conflict of interest.

Supplementary Information

Supplementary information is available at MP's website

Introduction

Norepinephrine has long been regarded as a stress neurotransmitter that can induce anxiety and changes in cardiovascular activity.[1, 2] Our understanding of the role of noradrenergic neurons in stress is derived from research that focuses primarily on locus coeruleus noradrenergic (LC-NE) neurons; however, other central NE neurons also provide a substantial input to stress-related brain regions.[3–10] Most studies suggest that these neurons, like those of the locus coeruleus, promote the stress response,[11–14] but there is some evidence that hints at an opposite role.[15, 16] These inconsistent and contradictory findings may result from heterogeneity among non-LC-NE neurons and the difficulty in reproducibly targeting these loosely-organized cells in the pons and medulla.

Strategies for targeting noradrenergic neurons based on molecular criteria[8] offer the possibility of reproducible experimental access to functionally relevant subgroupings that have been obscured by the anatomical classification previously used to study these neurons. We previously reported two subgroupings of noradrenergic neurons, each defined by developmental expression of specific transcription factors, that project to stress-related forebrain targets such as the basolateral amygdala (BLA) and BNST.[8] The first, defined by *En1 (En1*-LC neurons), includes the compact locus coeruleus. The second, defined by *Hoxb1* (*Hoxb1*-NE neurons),[8, 17] is scattered in the medulla and pons outside of the LC. In addition to their forebrain targets, *Hoxb1*-NE neurons also project to the LC, suggesting they may play a unique role in the regulation of stress.

Here, we test this hypothesis using an intersectional chemogenetic approach[18] to assess the behavioral and physiological effect of selectively activating *Hoxb1*-NE neurons. We found that direct activation of this population resulted in a more active response to acute stressors and reduced anxiety-like behavior. Consistent with this behavioral phenotype, functional MRI and Fos immunohistochemistry revealed reduced activity in some stress-related brain regions. Collectively, our results indicate that contrary to the general belief that activation of the noradrenergic system facilitates stress reactivity, *Hoxb1*-NE neurons have a distinct role in attenuating the behavioral response to acute stress.

Materials and Methods

Animals

All procedures related to the use of animals were approved by the National Institute of Environmental Health Sciences Animal Care and Use Committee and were in accordance with the National Institutes of Health guidelines for the care and use of laboratory animals. *Hoxb1*$^{tm1(cre)Og}$ (*Hoxb1*^{cre}),[19] *En1*$^{tm2(cre)Wrst}$ (*En1*^{cre}),[20] *Dbh*$^{tm1(Flpo)Pjen}$ (*Dbh*^{Flpo}),[8] *Gt(ROSA)26Sor*$^{tm3.2(CAG-EGFP,-CHRM3*/mCherry/Htr2a)Pjen}$ (*RC::FL-hM3Dq*),[18] and *Gt(ROSA)26Sor*$^{tm1.3(CAG-tdTomato,-EGFP)Pjen}$ (*RC::FLTG*)[21] mouse colonies are maintained on a C57BL/6J background. Male and female triple transgenic animals were generated by crossing *Hoxb1*^{cre} or *En1*^{cre} mice to double transgenic *Dbh*^{Flpo}*; RC::FL-hM3Dq* or *Dbh*^{Flpo}*; RC::FLTG* mice. Single- and double-transgenic littermates served as controls. All animals were group housed and maintained on a 12/12 h light-dark cycle with access to food and water *ad libitum*.

Tissue Collection

For timed matings, noon of the day a copulation plug was observed was designated as embryonic day (E) 0.5. E14.5 embryos were collected and immersion-fixed in 4% paraformaldehyde (PFA) in 0.01 M phosphate buffered saline (PBS) at 4 °C overnight. Following equilibration in 10%, 20%, and 30% sucrose in PBS, embryos were embedded in Tissue Freezing Medium (General Data Company, Cincinnati, OH), and 14 μm sagittal cryosections were mounted on Superfrost Plus microscope slides (Thermo Scientific, Waltham, MA), air dried and stored at −80 °C.

Adult mice were deeply anesthetized with sodium pentobarbital and perfused transcardially with PBS followed by 4% PFA. Brains and adrenals were postfixed overnight by immersion in 4% PFA at 4°C. Following a rinse in PBS, tissue was cryoprotected in 30% sucrose in PBS and embedded in Tissue Freezing Medium. 40 μm free-floating coronal brain sections were collected in PBS, transferred to a cryoprotectant and stored at −80 °C. 14 μm sagittal brain sections were collected on Superfrost Plus slides, air dried, and stored at −80 °C. Adrenals were sectioned at 20 μm and collected on Superfrost Plus slides, air dried and stored at −80 °C.

Immunohistochemistry and *in situ* hybridization

Immunofluorescent labeling was used to enhance signal from fluorescent proteins in fixed tissue. mCherry-expressing neurons were detected using Rat anti-mCherry primary antibody (1:1000; EST202, Kerafast, Boston, MA) and Goat anti-rat Alexa Fluor 568 secondary antibody (1:1000; A11077, Invitrogen, Carlsbad, CA). eGFP-expressing neurons and axons were detected using Chicken anti-GFP primary antibody (1:1000; AB13970, Abcam, Cambridge, MA) and Goat anti-chicken Alexa Fluor 488 secondary antibody (1:1000; A11039, Invitrogen). tdTomato-expressing neurons and fibers were detected using Rabbit anti-dsRed primary antibody (1:1000; 632496, Clontech Laboratories, Inc., Mountain View, CA) and Goat anti-rabbit Alexa Fluor 568 secondary antibody (1:1000; A11036, Invitrogen), or Rat anti-tdTomato primary antibody (1:2000; EST203, Kerafast) and Goat anti-rat Alexa Fluor 568 secondary antibody (1:1000; A11077, ThermoFisher Scientific, Waltham, MA). The noradrenergic identity of neurons was confirmed with Rabbit anti-TH primary antibody (1:1000; AB152, Millipore, Billerica, MA) and Goat anti-rabbit Alexa Fluor 633 secondary antibody (1:1000; A21071, Invitrogen). The noradrenergic identity of fibers was confirmed with Mouse anti-NET primary antibody (1:1000; 1447-NET, PhosphoSolutions, Aurora, CO) and Goat anti-mouse Alexa Fluor 633 secondary antibody (1:1000; A21052, Invitrogen). Fos was detected using a Rabbit anti-c-Fos primary antibody (1:2000; ab190289, Abcam) and Goat anti-rabbit Alexa Fluor 633 secondary antibody (1:1000; ThermoFisher Scientific). TrueBlack (Biotium, Fremont, CA) was applied in some experiments to reduce the level of autofluorescence.

For immunoperoxidase staining, Fos was detected using Rabbit anti-cFos primary antibody and a biotinylated Goat anti-rabbit secondary antibody (1:500, BA-1000, Vector Laboratories Inc., Burlingame, CA) used in conjunction with Vectastain Elite ABC kit and DAB substrate kit (Vector Labs) according to the manufacturer's instructions. To detect NE neurons in immunoperoxidase-stained sections containing the LC, we used chicken anti-TH

primary antibody (1:500; CH23006, Neuromics, Edina, MN) and biotinylated goat anti-chicken secondary antibody (1:500; BA-9010, Vector Labs) with Vectastain Elite ABC kit and Vector SG substrate kit (Vector Labs). *In situ* hybridization was performed using RNAscope probes (Advanced Cell Diagnostics, Newark, CA) for Mm-Pnmt-C3 (426421-C3), Mm-Gal-C3 (400961-C3), Mm-Penk-C3 (318761-C3), Mm-Npy-C3 (313321-C3) according to the manufacturer's instructions. Coverslips were applied with Vectashield hard set mounting medium with DAPI (H-1500, Vector Labs) or Prolong Diamond Antifade Mountant (P36970, Invitrogen) for fluorescently labeled slides, and with Permount (SP15–500, ThermoFisher Scientific) for immunoperoxidase-labeled slides.

Digital image processing

Images of immunofluorescently-labeled sections were collected using Zeiss LSM 710, 780, or 880 inverted confocal microscopes (Carl Zeiss Microscopy, Thornwood, NY). When necessary, Zen 2012 Black Software (Carl Zeiss) was used to convert z-stacks to maximum intensity projections. Images were modified only by adjusting brightness and contrast across the entire image to optimize the fluorescence signal. Anatomical location was confirmed by reference to a mouse brain atlas.[22] For Fos quantification, brightfield images of immunoperoxidase stained tissue were acquired using an Aperio AT2 slide scanner (Leica Biosystems Inc., Buffalo Grove, IL) with a 40× objective. Digital images were subsequently exported from Aperio Imagescope (Leica Biosystems) to FIJI software[23] as a tif or jpeg file for further analyses.

Cell counts

To quantify the number of *Hoxb1*-NE neurons in the subcoeruleus, A5, A1, and A2 nuclei, we labeled the mCherry- and EGFP-positive neurons using double immunofluorescence as described above. Cell numbers are the sum of unilateral counts from 14 μm sagittal sections spaced approximately 70 μm apart. We manually counted the cells in these noradrenergic nuclei for a total of 12 animals. The number of Fos-positive *Hoxb1*-NE neurons following forced swim was quantified using the same procedure (n=5–7 mice per group). All counts were conducted by an experimenter blinded to the treatment group. To determine the number of *Hoxb1*-NE neurons that express galanin, enkephalin, or neuropeptide Y, we used *in situ* hybridization in combination with immunofluorescence labeling for EGFP and tdTomato on hindbrain sections from *Hoxb1*^{cre}*; Dbh*^{Flpo}*; RC::FLTG* triple transgenic mice (n=2–3 mice per peptide). Unilateral counts of EGFP-labeled and EGFP/peptide-colabeled neurons were summed from 14-μm sagittal sections spaced approximately 140 μm apart. Quantification of Fos-positive neurons (n=4–6 mice per treatment group) was performed on 40 μm immunoperoxidase-stained coronal sections (every 4th section) in the following brain regions: medial prefrontal cortex (mPFC), caudate putamen (CPu), dorsal and ventral BNST (dBNST and vBNST), BLA, central amygdala (CeA), paraventricular nucleus of hypothalamus (PVN), lateral hypothalamus (LH), dorsomedial hypothalamus (DMH), ventromedial hypothalamus (VMH), and the locus coeruleus. The quantification was conducted by an experimenter blinded to the treatment group. FIJI software[23] was used to measure the region of interest and perform automatic counting. The number of positive neurons was then normalized to area (expressed as mm^2) for statistical analysis.

Slice preparation and electrophysiological recordings

Hoxb1-NE/hM3Dq and control mice (2–4 months old for cell-attached recording with no blockers, and 2–4 weeks old for cell-attached recording with blockers) were anesthetized with isoflurane and decapitated. Brains were quickly removed and placed into ice-cold cutting solution (110 mM sucrose, 60 mM NaCl, 3 mM KCl, 7 mM $MgCl_2$, 0.5 mM $CaCl_2$, 1.25 mM NaH_2PO_4, 28 mM $NaHCO_3$, 1 mM ascorbate, 3 mM Na pyruvate, and 5 mM glucose) saturated with oxygen ($95\%O_2/5\%CO_2$). Coronal vibratome slices (250–300 μm thick) through the brainstem containing the nucleus tractus solitarius (NTS) were collected into oxygenated artificial cerebrospinal fluid (aCSF) containing 126 mM NaCl, 3.5 mM KCl, 1.3 mM $MgCl_2$, 2 mM $CaCl_2$, 1.2 mM NaH_2PO_4, 25 mM $NaHCO_3$, and 10 mM glucose. After recovery at 34 °C for 30 minutes (min), the slices were kept at room temperature before recording.

A2 noradrenergic neurons that express either mCherry (*Hoxb1*-NE/hM3Dq) or EGFP (littermate controls) were identified by fluorescence under a 60× (NA 1.0) objective on a Nikon ECLIPSE FN1 microscope (Nikon Instruments Inc., Melvillle, NY) equipped with an iXon camera (Andor Technology Ltd., South Windsor, CT), Mosaic 3 imaging system (Andor Technology) and 545 nm X-Cite LED (Excelitas Technologies Corp., Waltham, MA). The recording patch-pipette was filled with aCSF and spikes were recorded in cell-attached loose-seal configuration to be minimally invasive and preserve G-protein-coupled signal transduction. Data were collected using an Axopatch 200B amplifier with Clampex 10.2 (Molecular Devices LLC, Sunnyvale, CA) and analyzed with Clampfit 10.2 (Molecular Devices). Neurons with positive responses to 25 mM KCl stimulation were tested for the effect of CNO (10 μM) applied via bath perfusion at a rate of 1.5–2 ml per min. For measurement of membrane potential change, tetrodotoxin (1 μM) and nimodipine (1 μM) were added to aCSF to block voltage-dependent Na^+ and Ca^{2+} channels respectively.

Behavioral tests and physiological measurements

All animals were tested during the light phase of the light-dark cycle. Adult male and female *Hoxb1*-NE/hM3Dq, *En1*-LC/hM3Dq, and littermate control mice were randomly assigned to receive i.p. injection of vehicle (0.6% DMSO in saline) or CNO (1 mg/kg). To allow direct comparison with *En1*-LC/hM3Dq mice, we timed CNO injection and testing to match our previously published protocols for the open field, light dark box, and elevated plus maze which show that effects of CNO can be detected 20–30 minutes post-injection.[18] The same cohort of *En1*-LC/hM3Dq and control mice was used for the forced swim and tail suspension test. Similarly, the same cohort of *Hoxb1*-NE/hM3Dq and control mice underwent the open field, light dark box, and elevated plus maze. A subset of *Hoxb1*-NE/hM3Dq and control mice used to measure body temperature was also used in measuring heart beat and the corticosterone level. If animals were used in more than one test, they were allowed at least 72 hours rest between each experiment. Details of the tests are described below.

Forced swim test.—To determine if *Hoxb1*-NE neurons respond to an acute stressor, *Hoxb1*-NE/hM3Dq mice were exposed to a forced swim for 6 min. During this time, mice were placed in a transparent cylinder (9.5 cm in diameter, height 44 cm; Noldus, Leesburg,

VA) filled with water (~22 °C, height 20 cm) and lit by white light. The control group of mice remained in their cages and did not undergo the forced swim. Two hours after the end of the forced swim exposure, tissue was collected and processed for Fos immunohistochemistry as described above.

To test whether activation of *Hoxb1*-NE and *En1*-LC neurons affects the response to the forced swim stress, mice were administered vehicle or CNO (1 mg/kg) 20 min prior to the test. As described above, mice were placed in a transparent cylinder filled with water for 6 min, during which time their behavior was recorded. Immobility, or floating behavior, is defined as the absence of directed movements of animals' head and body. The total time spent floating was later scored manually by an observer who was blind to the genotype and treatment of the animals. After the test, each mouse was dried completely before being returned to their home cages.

Tail suspension test.—This test was conducted in a test chamber (54 × 19 × 47 cm; Stoelting Co., Wood Dale, IL), and the session started 20 min after mice received an i.p. injection of vehicle or CNO. Each mouse was suspended by its tail for 6 min, and its behavior during this time was recorded. The immobility time, which is defined as the total duration that animal shows no movement, was later scored by an observer who was blind to the genotype and treatment of the animals.

Open field test.—Following i.p. injection of vehicle or CNO, mice were immediately placed in an unilluminated open arena (27 × 27 × 20 cm; Med Associates Inc., Fairfax, VT) and allowed to freely explore the arena for 90 min. Distance travelled during the 90-min period was recorded and analyzed.

Light dark box.—The test was conducted in an arena (27 × 27 × 20 cm, Med Associates) that was equally divided into two compartments (dark: 0 lux; light: ~980 lux). To test whether *Hoxb1*-NE activation affects the performance in the light dark box test, mice received an injection 20 min prior to the test and were allowed to freely explore both compartments for 10 min. To confirm that noradrenergic signaling underlies the behavioral changes induced by *Hoxb1*-NE stimulation, mice received two injections prior to the light dark box testing. The first injection was either a vehicle (1% DMSO in sterile water) or an adrenergic antagonist cocktail, which consists of prazosin (0.2 mg/kg, i.p.) and propranolol (5 mg/kg, i.p.). Thirty minutes afterwards, the mice received either vehicle or CNO (1 mg/kg, i.p.) injections. The mice were tested in the light dark box for 10 minutes, twenty minutes after the second injection. The time spent in the light compartment was recorded and analyzed.

Elevated plus maze.—Mice received vehicle or CNO 30 min prior to the test. At the start of the test, mice were placed on the center of a brightly illuminated '+' shaped maze (Stoelting Co.), which consists of two open arms (35 × 5 cm) and two closed arms (35 × 5 cm) elevated 50 cm above the floor. The test lasted 5 min, during which time the mice were allowed to freely explore the maze. The time spent in the open and closed arms, and the number of entries into the open and closed arms were recorded and later scored by an observer who was blind to the genotype and treatment of the animals. These measurements,

as well as the % time in the open arm (time in the open arm/time in the open and closed arms), were later used for analysis.

Heart rate measurement.—Heart rate was measured using the ECGenie system (Mouse Specifics, Inc., Framingham, MA). The electrocardiography (ECG) signals were detected through disposable footpad electrodes and digitized (16-bit precision) using a sampling rate of 2,000 samples per second. Each animal was allowed to acclimate to the platform for at least 15 min before the recording started. Following an i.p. injection of vehicle or CNO, the animals were placed back to the platform for an additional 40 min, during which time their ECG signals were monitored and recorded. For the analysis, 3–4 segments of continuous recordings (containing around 20–30 ECG signals) at 0–5 min, 20 min, 40 min time points were selected. These signals were analyzed using e-Mouse software (Mouse Specifics), which generated the heart rate data using the average of R-R interval. For each animal, the data were the average of at least 3 segments during individual time point and were expressed as beats per minute.

Body temperature measurement.—Mice were briefly restrained for baseline measurement of body temperature using a rectal probe (Physitemp Instruments, Clifton, NJ). Following i.p. injection of vehicle or CNO, body temperature was measured every 20 min for 60 min.

Blood collection and corticosterone measurement

Blood samples were collected via the submandibular vein, 20 min after mice received either vehicle or CNO (1 mg/kg, i.p.) injection during the light phase of the light-dark cycle. This timing was selected to be consistent with the time of day and dosing schedule of behavioral experiments. The serum was separated from the samples, and the corticosterone level was measured using an enzyme immunoassay kit (K014-H5, Arbor Assays, Ann Arbor, MI) according to the manufacturer's instructions.

Functional MRI

fMRI was performed on *Hoxb1*-NE/hM3Dq and control mice anesthetized with continuous flow of 0.7–1.0% isoflurane in medical air using a 9.4T/30 cm scanner with a BGA-9S gradient insert, a 72 mm volume transmitter, and a quadrature mouse brain receiver coil (Bruker BioSpin, Billerica, MA). Body temperature, ECG and respiratory rate were continuously monitored while scanning to ensure stable physiological conditions throughout the experiments. Carboxymethyl Dextran coated Iron Oxide Nanoparticles (CION) developed in-house were injected intravenously (30 mg Fe/kg) to achieve cerebral blood volume (CBV)-weighted fMRI to improve functional contrast to noise.[24–27] Single-shot gradient-echo echo-planar-imaging (bandwidth = 250 kHz, TR/TE = 3000/12 ms, matrix = 64 × 64, FOV = 1.92 cm^2, slice number = 26 and slice thickness = 0.3 mm) was used to image the entire brain at an isotropic resolution of 300 μm continuously every 3 seconds for 40 minutes, with a 1 mg/kg dose of CNO injected via intraperitoneal catheter 10 minutes after scanning onset. fMRI data from individual subjects were preprocessed using AFNI v. 16.0.01[28] and warped to a probabilistic anatomical atlas[29] using ANTs v.2.1.0–5.[30] Regions of interest (ROIs) were determined by first placing seeds on corresponding anatomical

structures[22] and parcellated into functional clusters. These ROIs were thresholded with a FDR corrected *P*-value ≤ 0.05. fMRI time-course data were detrended using a linear fit of the baseline period to correct for linear temporal drifts attributed to both the contrast agent washout from circulation and/or MR gradient heating. CBV changes were calculated[24, 25, 27, 31] for each ROI and a mean CBV percent change between baseline and post-CNO time-courses were compared between each scan for both *Hoxb1*-NE/hM3Dq and control mice.

Statistical analysis

All data are expressed as the mean ± standard error (SEM). When the data met the assumption of normal distribution (Shapiro-Wilk test for normality) and equal variances (Levene's test for homogeneity of variances), we used unpaired 2-tailed *t*-test, two-way or repeated measures ANOVA to determine the differences between groups. When the data were skewed or did not meet the assumptions, we either transformed the raw data before conducting unpaired *t*-test and ANOVA or used non-parametric tests such as Mann-Whitney U test for analysis. Significance was set at $P<0.05$ for all analyses. All statistical analyses were conducted using IBM SPSS Statistics 21.0 (IBM Corp., Armonk, NY) or JMP Pro v.13 (SAS Institute Inc., Cary, NC). Graphpad Prism 7 (GraphPad Software Inc., La Jolla, CA) and Microsoft Excel (Microsoft Corporation, Redmond, WA) were used to create graphs. The number of subjects and specific statistical analyses used in each experiment are indicated in the text, figure legends, and Supplementary Table 1. We did not use any statistical methods to predetermine sample sizes; however, our sample sizes are similar to those reported previously.

Results

Intersectional chemogenetic targeting of *Hoxb1*-NE neurons

To determine the role of *Hoxb1*-NE neurons in response to acute stressors, we employed an intersectional chemogenetic approach similar to the strategy previously used to interrogate *En1*-LC neurons.[18] We generated triple transgenic *Hoxb1^{cre}; Dbh^{Flpo}; RC::FL-hM3Dq* (*Hoxb1*-NE/hM3Dq) mice in which the excitatory G-protein-coupled receptor hM3Dq fused to mCherry is expressed in neurons with a shared history of *Hoxb1^{cre}* and the noradrenergic-specific driver *Dbh^{Flpo}*. All remaining NE neurons, with no history of *Hoxb1^{cre}* expression, are labelled with EGFP (Figure 1a–b). This strategy solves the problem of gaining selective experimental access to a neuronal population that is too widely dispersed for reliable viral targeting and which no longer expresses *Hoxb1* in the adult. In triple transgenic mice, we observed tyrosine hydroxylase+, hM3Dq-mCherry+ neurons intermingled with EGFP+ neurons in the dorsal and ventral subcoeruleus (SubCD and SubCV), A5, and caudal A1 and A2 noradrenergic nuclei, constituting approximately 17% of NE neurons in these nuclei (Figure 1b-c). In addition, we observed a small population of *Hoxb1*-NE neurons in the peripheral nervous system and adrenal medulla (Supplementary Figure 1).

To determine whether the synthetic hM3Dq ligand, clozapine-N-oxide (CNO), could activate hM3Dq-expressing *Hoxb1*-NE neurons, we performed cell-attached recordings on brain slices at the level of the caudal A2 noradrenergic nucleus. As expected, application of 10 μM

CNO significantly increased the frequency of action potentials in hM3Dq-mCherry-expressing neurons of *Hoxb1*-NE/hM3Dq mice (Wilcoxon signed ranks test, P=0.018), while having no effect in littermate controls (Wilcoxon signed ranks test, P=0.317) (Figure 1d-e). To eliminate network effects and oscillations, we next recorded in the presence of the Na^+ channel blocker tetrodotoxin (1 μM) and L-type Ca^{2+} channel blocker nimodipine (1 μM). Under this condition, bath application of CNO (10 μM) elicited a significant depolarization in hM3Dq-mCherry-expressing neurons (1.28 ± 0.43 mV) but had no effect on controls (0.11 ± 0.25 mV) (Difference between *Hoxb1*-NE/hM3Dq and controls: Mann-Whitney U test, P=0.030) (Supplementary Figure 2). Taken together, these data validate our chemogenetic strategy, confirming we can reliably manipulate the activity of *Hoxb1*-NE neurons.

In vivo activation of *Hoxb1*-NE neurons promotes an active response to acute stress

We first assessed whether *Hoxb1*-NE neurons are activated in response to an acute stressor by determining levels of Fos expression following a 6-minute forced swim, a well-established paradigm to induce stress.[32] We found a significant increase in Fos expression in *Hoxb1*-NE neurons of the subcoeruleus, compared to controls, following the forced swim stressor (unpaired *t*-test, P=0.033) (Figure 2a), confirming that the endogenous activity of this population is implicated in acute stress responses.

Next, we examined whether *in vivo* activation of *Hoxb1*-NE neurons affects how animals respond to acute stressors. Maladaptive response to stress is associated with psychological disorders such as depression,[33] and noradrenergic transmission has long been implicated in this process.[34, 35] To investigate the role of this non-LC population, *Hoxb1*-NE/hM3Dq and littermate control mice underwent the forced swim and tail suspension tests. Both are well-established paradigms to induce stress and assess the level of behavioral despair, and are commonly used to assess the effectiveness of antidepressants.[32, 36, 37] CNO-treated (1 mg/kg, i.p.) *Hoxb1*-NE/hM3Dq mice spent significantly less time immobile compared to vehicle-treated mice in both the forced swim (two-way ANOVA, genotype × treatment interaction: $F(1, 62)=7.132$, P=0.01) and tail suspension tests (two-way ANOVA, genotype × treatment interaction: $F(1, 53)=5.782$, P=0.02) (Figure 2b-c and Supplementary Figure 3).

The reduction of immobility induced by *Hoxb1*-NE activation cannot be attributed to mere change in locomotion, as there was no difference in the distance travelled by CNO-treated *Hoxb1*-NE/hM3Dq mice and controls in a 90-minute open field test (10-minute bin time course: repeated measures ANOVA, effect of treatment: $F(1, 20)= 0.507$, P=0.485; 90 min: two-way ANOVA, genotype × treatment interaction: $F(3, 58)=0.967$, P=0.414) (Figure 2d and Supplementary Figure 3). Furthermore, we observed no difference in distance travelled 21–26 minutes post-injection (two-way ANOVA, effect of treatment: $F(1, 58)=0.007$, P=0.932), which corresponds to the time frame of the forced swim and tail suspension tests (Supplementary Figure 3). These findings suggest that activation of *Hoxb1*-NE neurons mimics the effect of antidepressants and is sufficient to promote a more active response when facing an acute stressor.

Next, we used *En1*-LC/hM3Dq mice to directly compare the behavioral consequences of activating the LC during forced swim and tail suspension tests. In contrast to activation of

Hoxb1-NE neurons, activation of *En1*-LC neurons significantly increased immobility time in the forced swim test compared to controls (two-way ANOVA, effect of treatment: F(1, 48)=5.726, P=0.021). In the tail suspension test, there was no difference in immobility time between CNO- or vehicle-treated *En1*-LC/hM3Dq mice or their littermate controls (two-way ANOVA, effect of treatment: F(1, 46)=0.093, P=0.762) (Figure 2e-f). Taken together, these results suggest that *Hoxb1*- and LC-NE neurons play very different roles in an animal's response to acute stress.

In vivo activation of *Hoxb1*-NE neurons reduces anxiety-like behavior and heart rate

Acute stress can also evoke anxiety, a negative affective state characterized by a high level of arousal. LC-NE signaling is critical in driving this response.[1, 18] To investigate the role of *Hoxb1*-NE neurons in mediating this aspect of the stress response we tested *Hoxb1*-NE/hM3Dq mice and controls in the light dark box (LDB) and elevated plus maze (EPM). Chemoactivation of *Hoxb1*-NE neurons significantly increased the time spent in the more aversive light compartment of the LDB compared to controls (two-way ANOVA, effect of treatment: F(1, 62)= 3.043, P=0.086; *a priori* unpaired t-test in *Hoxb1*-NE/hM3Dq mice: t(20)=-2.139, P=0.045) (Figure 2g). Our results from the EPM further support an anxiolytic effect of *Hoxb1*-NE activation. As shown in Figure 2h, chemogenetic activation of *Hoxb1*-NE neurons significantly increased the number of entries into, and time spent exploring, the more aversive open arm of the EPM (entries: two-way ANOVA, effect of treatment: F(1, 56)= 4.629, P=0.036; percentage time: two-way ANOVA, effect of treatment: F(1, 56)= 7.773, P=0.007). There was no difference in total arm entries (two-way ANOVA, effect of treatment: F(1, 56)=0.000, P=0.995), or closed arm entries between vehicle- and CNO-treated *Hoxb1*-NE/hM3Dq mice (two-way ANOVA, effect of treatment: F(1, 56)= 5.612, P=0.021; post-hoc unpaired t-test: t(18)=0.651, P=0.523) (Supplementary Figure 4), indicating that the change in open arm entries was not due to nonspecific impairment in locomotion. However, there was a significant reduction in closed arm entries by CNO-treated controls, relative to vehicle-treated controls (post-hoc unpaired t-test: t(38)=3.282, P=0.002) (Supplementary Figure 4). Taken together, these data demonstrate that activation of *Hoxb1*-NE neurons results in decreased anxiety-like behavior. In contrast, our previous results showed that activation of *En1*-LC neurons elicits anxiety-like behavior in the EPM and LDB tests.[18] Thus, these two distinct populations may play opposite roles in anxiety-like behavior.

Physiological alterations such as increased heart rate constitute another hallmark response to stress mediated by the LC-NE system.[2] To evaluate the effect of *Hoxb1*-NE neuron activation on heart rate, we performed electrocardiogram recordings in conscious mice. We found that CNO significantly reduced the heart rate of *Hoxb1*-NE/hM3Dq mice for 40 minutes post-injection, while causing no change in littermate controls (repeated measures ANOVA, genotype × treatment × time interaction: F(2, 82)=5.007, P=0.009) (Figure 3a). Similar behavioral and physiological phenotypes can be induced by direct vagal stimulation, suggesting that our results could be mediated peripherally. To test this hypothesis, we examined two additional physiological changes associated with vagal nerve stimulation: decreased core temperature and increased corticosterone levels.[38–40] Upon *Hoxb1*-NE neuron activation we measured no change in either temperature or corticosterone levels

compared to controls (temperature: repeated measures ANOVA, effect of treatment: F(1, 78)=0.271, P=0.604; corticosterone: two-way ANOVA, effect of treatment: F(1, 50)=0.134, P=0.716) (Figure 3b and c). These results suggest that the behavioral and physiological phenomena observed upon *Hoxb1*-NE neuron activation are likely governed by the central noradrenergic system.

Noradrenergic signaling underlies the anxiolytic effect of *Hoxb1*-NE activation

We next wanted to know whether the anxiolytic response upon *Hoxb1*-NE neuron activation was dependent on NE. Noradrenergic neurons are known to coexpress a variety of neuropeptides, which can not only modulate their activity, but also play a prominent role in regulating stress responses. Several of these stress-related neuropeptides—such as galanin, enkephalin, and neuropeptide Y (NPY)—are found in noradrenergic nuclei outside of the LC,[5, 41] raising the possibility that the phenotypes observed upon *Hoxb1*-NE activation are not mediated by NE. To address this question, we assessed the performance of *Hoxb1*-NE/hM3Dq mice in the LDB after administration of a cocktail of adrenergic antagonists (prazosin, 0.2 mg/kg, i.p. and propranolol, 5 mg/kg, i.p.) or vehicle (1% DMSO in sterile water) followed by CNO (1 mg/kg, i.p.) or vehicle (Supplementary Figure 5a). While chemogenetic activation of *Hoxb1*-NE neurons significantly increased time spent exploring the light compartment during the 10-minute test, this effect was eliminated in mice pre-administered prazosin and propranolol (two-way ANOVA, effect of CNO: F(1, 29)=1.057, P=0.312; *a priori* unpaired t-test between vehicle-vehicle and vehicle-CNO treated mice: t(15)=-2.297, P=0.036; *a priori* unpaired t-test between adrenergic antagonist-vehicle and adrenergic antagonist-CNO treated mice: t(14)=0.089, P=0.930) (Supplementary Figure 5b-c). Overall, these results suggest that noradrenergic signaling through α1 and β adrenoceptors is required for the *Hoxb1*-NE-induced anxiolytic responses. However, these experiments do not rule out a modulatory role for co-expressed neuropeptides.

To further investigate this question, we asked if neuropeptides implicated in stress regulation are expressed in *Hoxb1*-NE neurons. Using our dual recombinase-responsive indicator allele (*RC::FLTG*) to label *Hoxb1*-NE neurons with EGFP and all other NE neurons with tdTomato,[21] we determined the number of *Hoxb1*-NE neurons expressing Gal, Enk, or Npy mRNA. While Gal- and Enk-expressing neurons were observed throughout the hindbrain, very few *Hoxb1*-NE neurons expressed these neuropeptides (Supplementary Figure 5d-e). In contrast, approximately 46% of *Hoxb1*-NE neurons in the A1 nucleus, and 15% in the A2 nucleus expressed NPY (Supplementary Figure 5f). Taken together, these results suggest that while noradrenergic transmission is required for the anxiolytic effect induced by *Hoxb1*-NE neurons, corelease of NPY on central targets may also play a role in this process.

In vivo activation of *Hoxb1*-NE neurons reduces neuronal activity in stress-related brain regions

Hoxb1-NE neurons provide a substantial input to stress-related targets, including regions of the BNST, amygdala, hypothalamus and locus coeruleus.[8] However, it is unclear if *Hoxb1*-NE inputs to these regions are topographically distinct from those of other NE populations, including the locus coeruleus. To address this question, we used our dual recombinase-responsive indicator allele (*RC::FLTG*) that is capable of labeling projections from two

neuronal populations simultaneously (Figure 4a).[21] In this experiment *Hoxb1*-NE neurons and their axons were labelled with EGFP, while all other NE neurons were labeled with tdTomato. Noradrenergic identity of labeled axons was confirmed using an antibody against the norepinephrine transporter (NET; data not shown). We observed no obvious topographical segregation of NE inputs. *Hoxb1*-NE axons were observed in the LC and peri-LC dendritic field (Figure 4b), and closely intermingled with those of other NE neurons at stress related regions of the forebrain (Figure 4c-h).

To investigate the effects of *Hoxb1*-NE activation on these central targets, we monitored brain activity changes using cerebral blood volume (CBV)-weighted fMRI.[26] Upon administration of CNO (1 mg/kg, i.p.), we observed a significant reduction in CBV in the ventral BNST, amygdala, and the locus coeruleus of *Hoxb1*-NE/hM3Dq mice compared to their controls (unpaired *t*-test, P=0.012, 0.001, and 0.006, respectively) (Figure 5a-e, g), suggesting that activation of *Hoxb1*-NE neurons reduced activity in these regions. The phenomena observed here were not caused by global CBV changes, as no difference was observed in the caudate putamen, a region that does not receive inputs from *Hoxb1*-NE neurons (unpaired *t*-test, P=0.653) (Figure 5f and g). To confirm that *Hoxb1*-NE activation results in decreased activation of specific target regions, we next examined Fos immunoreactivity. We found that CNO activation of *Hoxb1*-NE neurons leads to a significant reduction in Fos expression in the ventral BNST (unpaired *t*-test, P=0.018), with a trend of reduction in the dorsal BNST, BLA and LC (unpaired *t*-test, P=0.076, 0.078, and 0.076, respectively) (Supplementary Figure 6a-b). We observed no difference in various hypothalamic regions, including the PVN, LH, DMH, or VMH (unpaired *t*-test or Mann-Whitney U test, P=0.992, 0.444, 0.257, and 0.358, respectively) (Supplementary Figure 6c). In addition, we did not find any change in Fos expression in the medial prefrontal cortex and the caudate putamen (unpaired *t*-test, P=0.520 and 0.530, respectively), two regions that receive no *Hoxb1*-NE inputs, indicating that the reduction in Fos was specific to direct *Hoxb1*-NE activation (Supplementary Figure 6c). These data demonstrate that activation of *Hoxb1*-NE neurons results in decreased activity in stress-related target regions.

Discussion

Our results reveal a role for *Hoxb1*-NE neurons in attenuating the behavioral response to acute stress. The forced swim and tail suspension tests suggest that activation of *Hoxb1*-NE neurons is sufficient to promote a more active coping response during acute stress, mimicking the effects of antidepressants. In addition, results from the LDB and EPM indicate that activation of *Hoxb1*-NE neurons results in decreased anxiety-like behavior. These results stand in contrast to our data from activating *En1*-LC neurons and previous reports demonstrating that increased activity of LC-NE neurons facilitates passive stress coping responses[42–44] and induces anxiety-like behavior.[1, 18] Together with our observation that multiple stress-related forebrain regions show reduced neuronal activity upon *Hoxb1*-NE activation, the behavioral data indicate that this relatively small population of neurons attenuates the response to acute stressors, a role that appears to be very different from that of LC-NE system.

The mechanisms that mediate the differential effects of *Hoxb1*-NE and *En1*-LC neurons during acute stress are yet to be determined, but one potentially relevant factor is their differential peptide expression. We found that a subset of *Hoxb1*-NE neurons co-express NPY, a peptide known to promote stress coping and resilience.[45] While the anxiolytic response induced by *Hoxb1*-NE activation is blocked with adrenergic antagonists, NPY may nevertheless modulate noradrenaline transmission[46–48] and facilitate the "anti-stress" responses observed in the current study. Unlike the LC, where approximately 80% of NE neurons express galanin,[1, 49–51] we observed virtually no galanin expression in *Hoxb1*-NE neurons.

Another factor contributing to the differential effects of *Hoxb1*-NE and *En1*-LC activation may be their efferent projections. At target regions where *Hoxb1*-NE and *En1*-LC neurons share inputs, their axons are notably different in morphology and density.[8] *Hoxb1*-NE axons are considerably thicker with larger varicosities compared to *En1*-LC axons, and targets receiving dense inputs from *Hoxb1*-NE neurons receive sparse inputs from *En1*-LC and vice versa. The significance of these differences is currently unclear. In the current study we did not observe any obvious topographical segregation of *Hoxb1*-NE inputs to stress-related targets, when viewed in the context of all other noradrenergic inputs. A detailed analysis of these inputs–including identification of the target cells, the nature of the synapse, and adrenergic receptor expression–will likely provide further clues. For example, different adrenoceptors may be engaged, thus exerting their unique actions on synaptic transmission, [52] depending on their distribution at the target and the time scale and level of NE release from *Hoxb1*-NE and *En1*-LC neurons. Indeed, it is well-established that NE has different affinity for alpha 1, 2, and beta receptors, and there is evidence that the effect of NE on synaptic transmission in the BNST is dependent on the duration of NE application.[53, 54]

In addition to sharing inputs to a number of stress-related targets, these two noradrenergic populations also exhibit notable differences in their projection patterns. Unlike *En1*-LC neurons, *Hoxb1*-NE neurons do not project to the hippocampus or medial prefrontal cortex, two regions known to be involved in stress regulation. However, *Hoxb1*-NE neurons do provide a substantial input to the LC and peri-LC dendritic field, positioning them to directly modulate LC activity. Consistent with this idea, our fMRI and Fos results indicate reduced LC activity upon *Hoxb1*-NE activation. It well-established that the LC is activated by a variety of stressors (reviewed in[55]), and it is possible that *Hoxb1*-NE activation occurs in response to stress-induced *En1*-LC activation, serving to counteract the response to stress. Future experiments that measure both the timing and magnitude of *En1*-LC and *Hoxb1*-NE responses to the same stressors may shed light on these questions. Our inability to directly examine the consequence of *Hoxb1*-NE activation on LC activity, or any other target, represents a limitation of the current study. The mouse line employed here restricts expression of hM3Dq receptors to the cell body and dendrites,[18] precluding the possibility of target site-specific infusion of CNO. Unfortunately, the lack of $Hoxb1^{cre}$ expression in adult *Hoxb1*-NE neurons and their scattered distribution rules out the use of viral constructs for optogenetics. Furthermore, the currently available cre/flp-responsive optogenetic transgenes do not express at high enough levels.

These same limitations also prevent us from directly determining whether *Hoxb1*-NE neurons act in unison or mediate distinct aspects of the “anti-stress” response. A first step in addressing this question will require a detailed analysis, using retrograde beads or other labeling strategies, to identify which *Hoxb1*-NE neurons project to specific targets. Taking advantage of a mouse line expressing Cre in the pontine portion of the *Hoxb1* domain,[56] we have previously reported that *Hoxb1*-NE neurons located in the pontine SubC and/or A5 nuclei share some inputs with those located in the medullary A1 and/or A2 nuclei, including inputs to the BNST, PVN, DMH, LH and LC. Notably, only the medullary *Hoxb1*-NE neurons project to the BLA and CeA.[17]

What is clear from our previous and current results is that *Hoxb1*-NE neurons are heterogeneous. While a portion of *Hoxb1*-NE neurons in the A1 and A2 nuclei co-localized with NPY, this co-expression was not observed in the A5 or SubC. Moreover, the only significant increase in Fos following a swim stress was in *Hoxb1*-NE neurons residing in the SubC. This diversity within the *Hoxb1*-NE population may very likely reflect important functional differences. One possibility is that the degree to which the *Hoxb1*-NE population is activated depends on the duration and intensity of the stressor. Numerous studies have shown that different neural mechanisms are engaged in response to acute versus long-term stress and stressors of different magnitudes.[57, 58] In the current study we focused on acute effects of *Hoxb1*-NE activation and employed paradigms intended to measure the animals’ responses during a mildly stressful event. Therefore, future studies examining how *Hoxb1*-NE neurons modulate responses to chronic stress or more severe stressors will likely provide additional insight into the role of *Hoxb1*-NE in the stress response.

While the current study focused on direct comparison of *Hoxb1*-NE and *En1*-LC neurons, our results also imply functional heterogeneity within the anatomically defined noradrenergic nuclei (SubC, A5, A2 and A1) in which *Hoxb1*-NE neurons reside and form a minority subpopulation. Studies have shown that A1, A2, A5 are all responsive to varied stressors.[5] There is limited data on the role of SubC in stress; however, a recent study has identified a large number of TH+ presympathetic-premotor neurons within the SubC.[59] As these neurons are thought to integrate different systems in response to stress exposure,[60] this observation highlights the potential importance of SubC in stress regulation. The prevailing view, based primarily on investigation of A1 and A2 neurons, is that these anatomically defined nuclei play a role in promoting the stress response.[14, 61, 62] Thus, our current finding that activation of the *Hoxb1*-NE subpopulation attenuates the stress response suggests that these anatomically defined nuclei contain functionally distinct subpopulations. As the field moves beyond the study of NE neurons based solely on their anatomical location and begins to define these neurons using molecular and circuit-based criteria, we will likely uncover additional heterogeneity within the system, similar to heterogeneity that has been recently uncovered in the LC.[8, 63–71] The fact that many target regions receive inputs from multiple functionally distinct noradrenergic subpopulations—which likely vary in their responses to different stimuli, and intensity and timing of norepinephrine release—argues for caution when using genetic or pharmacological means to manipulate the noradrenergic system as a whole, or when targeting specific brain regions innervated by more than one noradrenergic subpopulation.

Finally, given that our conclusions rely on results of chemogenetic experiments, it is important to consider recent reports demonstrating that CNO is metabolized to clozapine.[72, 73] These reports, in conjunction with mouse studies demonstrating decreased endogenous NE levels 90 minutes after a single dose of ≥10 mg/kg of clozapine[74] and decreased membrane surface levels of the NE transporter one-hour post administration of 30 mg/kg of clozapine,[75] highlight the importance of using a relatively low dose of CNO, and including proper controls in chemogenetic experiments. In the current study, we administered CNO and vehicle to both hM3Dq-expressing mice and hM3Dq-negative controls. In the EPM we noted a significant reduction in closed arm entries by CNO-treated controls, relative to vehicle-treated controls. No effect of CNO in controls was observed in any other behavioral endpoint. All remaining behavior effects were only observed in CNO-treated hM3Dq-expressing mice, validating the specificity of our chemogenetic approach.

Conclusions

Our findings indicate that direct activation of *Hoxb1*-NE neurons decreases anxiety-like behavior and promotes an active coping response during acute stress, effects that are drastically different from the well-documented functions of the noradrenergic locus coeruleus. These observations contrast with the general belief that noradrenergic signaling promotes the stress response, and clearly demonstrate that the noradrenergic system constitutes multiple functional subpopulations.

Supplementary Material

Refer to Web version on PubMed Central for supplementary material.

Acknowledgments

Valuable support was provided by the NIEHS Comparative Medicine Branch, Biostatistics and Computational Biology Branch, Neurobehavioral Core and Fluorescence Microscopy and Imaging Core. We thank the NIDA Drug Supply Program for providing the CNO. This research was supported by the Intramural Research Program of the US National Institutes of Health, National Institute of Environmental Health Sciences (ZIA-ES102805 to P.J. and ZIA-ES090089–21 to J.L.Y.), and the Extramural Research Programs of the National Institute of Mental Health (R01MH111429, R41MH113252, R21MH106939) and National Institute of Neurological Disorders and Stroke (R01NS091236) to Y.Y.I.S.

References

1. McCall JG, Al-Hasani R, Siuda ER, Hong DY, Norris AJ, Ford CP et al. CRH Engagement of the Locus Coeruleus Noradrenergic System Mediates Stress-Induced Anxiety. Neuron 2015; 87(3): 605–620. [PubMed: 26212712]
2. Wood CS, Valentino RJ, Wood SK. Individual differences in the locus coeruleus-norepinephrine system: Relevance to stress-induced cardiovascular vulnerability. Physiol Behav 2017; 172: 40–48. [PubMed: 27423323]
3. Delfs JM, Zhu Y, Druhan JP, Aston-Jones G. Noradrenaline in the ventral forebrain is critical for opiate withdrawal-induced aversion. Nature 2000; 403(6768): 430–434. [PubMed: 10667795]
4. Flak JN, Myers B, Solomon MB, McKlveen JM, Krause EG, Herman JP. Role of paraventricular nucleus-projecting norepinephrine/epinephrine neurons in acute and chronic stress. Eur J Neurosci 2014; 39(11): 1903–1911. [PubMed: 24766138]
5. Kvetnansky R, Sabban EL, Palkovits M. Catecholaminergic systems in stress: structural and molecular genetic approaches. Physiol Rev 2009; 89(2): 535–606. [PubMed: 19342614]

6. Petrov T, Krukoff TL, Jhamandas JH. Branching projections of catecholaminergic brainstem neurons to the paraventricular hypothalamic nucleus and the central nucleus of the amygdala in the rat. Brain Res 1993; 609(1–2): 81–92. [PubMed: 8099526]
7. Reyes BA, Van Bockstaele EJ. Divergent projections of catecholaminergic neurons in the nucleus of the solitary tract to limbic forebrain and medullary autonomic brain regions. Brain Res 2006; 1117(1): 69–79. [PubMed: 16962080]
8. Robertson SD, Plummer NW, de Marchena J, Jensen P. Developmental origins of central norepinephrine neuron diversity. Nat Neurosci 2013; 16(8): 1016–1023. [PubMed: 23852112]
9. Sawchenko PE, Swanson LW. The organization of noradrenergic pathways from the brainstem to the paraventricular and supraoptic nuclei in the rat. Brain Res 1982; 257(3): 275–325. [PubMed: 6756545]
10. Shin JW, Geerling JC, Loewy AD. Inputs to the ventrolateral bed nucleus of the stria terminalis. J Comp Neurol 2008; 511(5): 628–657. [PubMed: 18853414]
11. Bundzikova-Osacka J, Ghosal S, Packard BA, Ulrich-Lai YM, Herman JP. Role of nucleus of the solitary tract noradrenergic neurons in post-stress cardiovascular and hormonal control in male rats. Stress 2015; 18(2): 221–232. [PubMed: 25765732]
12. Cecchi M, Khoshbouei H, Javors M, Morilak DA. Modulatory effects of norepinephrine in the lateral bed nucleus of the stria terminalis on behavioral and neuroendocrine responses to acute stress. Neuroscience 2002; 112(1): 13–21. [PubMed: 12044468]
13. Cecchi M, Khoshbouei H, Morilak DA. Modulatory effects of norepinephrine, acting on alpha 1 receptors in the central nucleus of the amygdala, on behavioral and neuroendocrine responses to acute immobilization stress. Neuropharmacology 2002; 43(7): 1139–1147. [PubMed: 12504920]
14. Zheng H, Rinaman L. Yohimbine anxiogenesis in the elevated plus maze requires hindbrain noradrenergic neurons that target the anterior ventrolateral bed nucleus of the stria terminalis. Eur J Neurosci 2013; 37(8): 1340–1349. [PubMed: 23368289]
15. Cryan JF, Page ME, Lucki I. Noradrenergic lesions differentially alter the antidepressant-like effects of reboxetine in a modified forced swim test. Eur J Phamacol 2002; 436(3): 197–205.
16. Daubert DL, McCowan M, Erdos B, Scheuer DA. Nucleus of the solitary tract catecholaminergic neurons modulate the cardiovascular response to psychological stress in rats. J Physiol 2012; 590(19): 4881–4895. [PubMed: 22753543]
17. Robertson SD, Plummer NW, Jensen P. Uncovering diversity in the development of central noradrenergic neurons and their efferents. Brain Res 2016; 1641(Pt B): 234–244. [PubMed: 26612521]
18. Sciolino NR, Plummer NW, Chen YW, Alexander GM, Robertson SD, Dudek SM et al. Recombinase-Dependent Mouse Lines for Chemogenetic Activation of Genetically Defined Cell Types. Cell Rep 2016; 15(11): 2563–2573. [PubMed: 27264177]
19. O'Gorman S Second branchial arch lineages of the middle ear of wild-type and Hoxa2 mutant mice. Dev Dyn 2005; 234(1): 124–131. [PubMed: 15861402]
20. Kimmel RA, Turnbull DH, Blanquet V, Wurst W, Loomis CA, Joyner AL. Two lineage boundaries coordinate vertebrate apical ectodermal ridge formation. Genes Dev 2000; 14(11): 1377–1389. [PubMed: 10837030]
21. Plummer NW, Evsyukova IY, Robertson SD, de Marchena J, Tucker CJ, Jensen P. Expanding the power of recombinase-based labeling to uncover cellular diversity. Development 2015; 142(24): 4385–4393. [PubMed: 26586220]
22. Paxinos G, Franklin KBJ. The Mouse Brain in Sterotaxic Coordinates. Academic Press: San Diego, CA, 2013.
23. Schindelin J, Arganda-Carreras I, Frise E, Kaynig V, Longair M, Pietzsch T et al. Fiji: an open-source platform for biological-image analysis. Nat Methods 2012; 9(7): 676–682. [PubMed: 22743772]
24. Albaugh DL, Salzwedel A, Van Den Berge N, Gao W, Stuber GD, Shih YY. Functional Magnetic Resonance Imaging of Electrical and Optogenetic Deep Brain Stimulation at the Rat Nucleus Accumbens. Sci Rep 2016; 6: 31613. [PubMed: 27601003]

25. Decot HK, Namboodiri VM, Gao W, McHenry JA, Jennings JH, Lee SH et al. Coordination of Brain-Wide Activity Dynamics by Dopaminergic Neurons. Neuropsychopharmacology 2017; 42(3): 615–627. [PubMed: 27515791]
26. Mandeville JB, Jenkins BG, Chen YC, Choi JK, Kim YR, Belen D et al. Exogenous contrast agent improves sensitivity of gradient-echo functional magnetic resonance imaging at 9.4 T. Magn Reson Med 2004; 52(6): 1272–1281. [PubMed: 15562489]
27. Van Den Berge N, Albaugh DL, Salzwedel A, Vanhove C, Van Holen R, Gao W et al. Functional circuit mapping of striatal output nuclei using simultaneous deep brain stimulation and fMRI. NeuroImage 2017; 146: 1050–1061. [PubMed: 27825979]
28. Cox RW. AFNI: software for analysis and visualization of functional magnetic resonance neuroimages. Comput Biomed Res 1996; 29(3): 162–173. [PubMed: 8812068]
29. Ullmann JF, Watson C, Janke AL, Kurniawan ND, Reutens DC. A segmentation protocol and MRI atlas of the C57BL/6J mouse neocortex. NeuroImage 2013; 78: 196–203. [PubMed: 23587687]
30. Avants BB, Tustison NJ, Song G, Cook PA, Klein A, Gee JC. A reproducible evaluation of ANTs similarity metric performance in brain image registration. NeuroImage 2011; 54(3): 2033–2044. [PubMed: 20851191]
31. Mandeville JB, Jenkins BG, Kosofsky BE, Moskowitz MA, Rosen BR, Marota JJ. Regional sensitivity and coupling of BOLD and CBV changes during stimulation of rat brain. Magn Reson Med 2001; 45(3): 443–447. [PubMed: 11241702]
32. Porsolt RD, Le Pichon M, Jalfre M. Depression: a new animal model sensitive to antidepressant treatments. Nature 1977; 266(5604): 730–732. [PubMed: 559941]
33. Chrousos GP, Gold PW. The concepts of stress and stress system disorders. Overview of physical and behavioral homeostasis. JAMA 1992; 267(9): 1244–1252. [PubMed: 1538563]
34. Bangasser DA, Valentino RJ. Sex differences in stress-related psychiatric disorders: neurobiological perspectives. Front Neuroendocrinol 2014; 35(3): 303–319. [PubMed: 24726661]
35. Chandley MJ, Ordway GA. Noradrenergic Dysfunction in Depression and Suicide In: Dwivedi Y (ed). The Neurobiological Basis of Suicide. CRC Press: Boca Raton, FL, 2012.
36. Cryan JF, Mombereau C. In search of a depressed mouse: utility of models for studying depression-related behavior in genetically modified mice. Mol Psychiatry 2004; 9(4): 326–357. [PubMed: 14743184]
37. Cryan JF, Mombereau C, Vassout A. The tail suspension test as a model for assessing antidepressant activity: review of pharmacological and genetic studies in mice. Neurosci Biobehav 2005; 29(4–5): 571–625.
38. De Herdt V, Puimege L, De Waele J, Raedt R, Wyckhuys T, El Tahry R et al. Increased rat serum corticosterone suggests immunomodulation by stimulation of the vagal nerve. J Neuroimmunol 2009; 212(1–2): 102–105. [PubMed: 19446345]
39. Hosoi T, Okuma Y, Nomura Y. Electrical stimulation of afferent vagus nerve induces IL-1beta expression in the brain and activates HPA axis. Am J Physiol Regul Integr Comp Physiol 2000; 279(1): R141–147. [PubMed: 10896875]
40. Larsen LE, Lysebettens WV, Germonpre C, Carrette S, Daelemans S, Sprengers M et al. Clinical Vagus Nerve Stimulation Paradigms Induce Pronounced Brain and Body Hypothermia in Rats. Int J Neural Syst 2017; 27(5): 1750016. [PubMed: 28178853]
41. Rinaman L Hindbrain noradrenergic A2 neurons: diverse roles in autonomic, endocrine, cognitive, and behavioral functions. Am J Physiol Regul Integr Comp Physiol 2011; 300(2): R222–235. [PubMed: 20962208]
42. Lin Y, Sarfraz Y, Jensen A, Dunn AJ, Stone EA. Participation of brainstem monoaminergic nuclei in behavioral depression. Pharmacol Biochem Behav 2011; 100(2): 330–339. [PubMed: 21893082]
43. Simson PG, Weiss JM, Hoffman LJ, Ambrose MJ. Reversal of behavioral depression by infusion of an alpha-2 adrenergic agonist into the locus coeruleus. Neuropharmacology 1986; 25(4): 385–389. [PubMed: 3012399]
44. Weiss JM, Simson PG, Hoffman LJ, Ambrose MJ, Cooper S, Webster A. Infusion of adrenergic receptor agonists and antagonists into the locus coeruleus and ventricular system of the brain.

Effects on swim-motivated and spontaneous motor activity. Neuropharmacology 1986; 25(4): 367–384. [PubMed: 2872608]

45. Sah R, Geracioti TD. Neuropeptide Y and posttraumatic stress disorder. Mol Psychiatry 2013; 18(6): 646–655. [PubMed: 22801411]
46. Finta EP, Regenold JT, Illes P. Depression by neuropeptide Y of noradrenergic inhibitory postsynaptic potentials of locus coeruleus neurones. Naunyn Schmiedebergs Arch Pharmacol 1992; 346(4): 472–474. [PubMed: 1436133]
47. Illes P, Finta EP, Nieber K. Neuropeptide Y potentiates via Y2-receptors the inhibitory effect of noradrenaline in rat locus coeruleus neurones. Naunyn Schmiedebergs Arch Pharmacol 1993; 348(5): 546–548. [PubMed: 8114954]
48. Singh C, Rihel J, Prober DA. Neuropeptide Y Regulates Sleep by Modulating Noradrenergic Signaling. Curr Biol 2017; 27(24): 3796–3811.e3795. [PubMed: 29225025]
49. Holets VR, Hokfelt T, Rokaeus A, Terenius L, Goldstein M. Locus coeruleus neurons in the rat containing neuropeptide Y, tyrosine hydroxylase or galanin and their efferent projections to the spinal cord, cerebral cortex and hypothalamus. Neuroscience 1988; 24(3): 893–906. [PubMed: 2454419]
50. Melander T, Hokfelt T, Rokaeus A, Cuello AC, Oertel WH, Verhofstad A et al. Coexistence of galanin-like immunoreactivity with catecholamines, 5-hydroxytryptamine, GABA and neuropeptides in the rat CNS. J Neurosci 1986; 6(12): 3640–3654. [PubMed: 2432203]
51. Perez SE, Wynick D, Steiner RA, Mufson EJ. Distribution of galaninergic immunoreactivity in the brain of the mouse. J Comp Neurol 2001; 434(2): 158–185. [PubMed: 11331523]
52. Daniel SE, Rainnie DG. Stress Modulation of Opposing Circuits in the Bed Nucleus of the Stria Terminalis. Neuropsychopharmacology 2016; 41(1): 103–125. [PubMed: 26096838]
53. Flavin SA, Winder DG. Noradrenergic control of the bed nucleus of the stria terminalis in stress and reward. Neuropharmacology 2013; 70: 324–330. [PubMed: 23466330]
54. McElligott ZA, Winder DG. Alpha1-adrenergic receptor-induced heterosynaptic long-term depression in the bed nucleus of the stria terminalis is disrupted in mouse models of affective disorders. Neuropsychopharmacology 2008; 33(10): 2313–2323. [PubMed: 18046308]
55. Valentino RJ, Van Bockstaele E. Convergent regulation of locus coeruleus activity as an adaptive response to stress. Eur J Pharmacol 2008; 583: 194–203. [PubMed: 18255055]
56. Di Bonito M, Narita Y, Avallone B, Sequino L, Mancuso M, Andolfi G et al. Assembly of the auditory circuitry by a Hox genetic network in the mouse brainstem. PLoS Genet 2013; 9(2): e1003249. [PubMed: 23408898]
57. McEwen BS, Bowles NP, Gray JD, Hill MN, Hunter RG, Karatsoreos IN et al. Mechanisms of stress in the brain. Nat Neurosci 2015; 18(10): 1353–1363. [PubMed: 26404710]
58. Russo SJ, Murrough JW, Han MH, Charney DS, Nestler EJ. Neurobiology of resilience. Nat Neurosci 2012; 15(11): 1475–1484. [PubMed: 23064380]
59. Nam H, Kerman IA. Distribution of catecholaminergic presympathetic-premotor neurons in the rat lower brainstem. Neuroscience 2016; 324: 430–445. [PubMed: 26946268]
60. Kerman IA, Bernard R, Rosenthal D, Beals J, Akil H, Watson SJ. Distinct populations of presympathetic-premotor neurons express orexin or melanin-concentrating hormone in the rat lateral hypothalamus. J Comp Neurol 2007; 505(5): 586–601. [PubMed: 17924541]
61. Banihashemi L, Rinaman L. Noradrenergic inputs to the bed nucleus of the stria terminalis and paraventricular nucleus of the hypothalamus underlie hypothalamic-pituitary-adrenal axis but not hypophagic or conditioned avoidance responses to systemic yohimbine. J Neurosci 2006; 26(44): 11442–11453. [PubMed: 17079674]
62. Myers B, Scheimann JR, Franco-Villanueva A, Herman JP. Ascending mechanisms of stress integration: Implications for brainstem regulation of neuroendocrine and behavioral stress responses. Neurosci Biobehav Rev 2017; 74(Pt B): 366–375. [PubMed: 27208411]
63. Chandler DJ, Gao WJ, Waterhouse BD. Heterogeneous organization of the locus coeruleus projections to prefrontal and motor cortices. Proc Natl Acad Sci USA 2014; 111(18): 6816–6821. [PubMed: 24753596]

64. Hirschberg S, Li Y, Randall A, Kremer EJ, Pickering AE. Functional dichotomy in spinal- vs prefrontal-projecting locus coeruleus modules splits descending noradrenergic analgesia from ascending aversion and anxiety in rats. eLife 2017; 6: e29808. [PubMed: 29027903]

65. Li Y, Hickey L, Perrins R, Werlen E, Patel AA, Hirschberg S et al. Retrograde optogenetic characterization of the pontospinal module of the locus coeruleus with a canine adenoviral vector. Brain Res 2016; 1641(Pt B): 274–290. [PubMed: 26903420]

66. McCall JG, Siuda ER, Bhatti DL, Lawson LA, McElligott ZA, Stuber GD et al. Locus coeruleus to basolateral amygdala noradrenergic projections promote anxiety-like behavior. eLife 2017; 6: e18247. [PubMed: 28708061]

67. Plummer NW, Scappini EL, Smith KG, Tucker CJ, Jensen P. Two Subpopulations of Noradrenergic Neurons in the Locus Coeruleus Complex Distinguished by Expression of the Dorsal Neural Tube Marker Pax7. Front Neuroanat 2017; 11: 60. [PubMed: 28775681]

68. Schwarz LA, Miyamichi K, Gao XJ, Beier KT, Weissbourd B, DeLoach KE et al. Viral-genetic tracing of the input-output organization of a central noradrenaline circuit. Nature 2015; 524(7563): 88–92. [PubMed: 26131933]

69. Uematsu A, Tan BZ, Johansen JP. Projection specificity in heterogeneous locus coeruleus cell populations: implications for learning and memory. Learn Mem 2015; 22(9): 444–451. [PubMed: 26330494]

70. Uematsu A, Tan BZ, Ycu EA, Cuevas JS, Koivumaa J, Junyent F et al. Modular organization of the brainstem noradrenaline system coordinates opposing learning states. Nat Neurosci 2017; 20(11): 1602–1611. [PubMed: 28920933]

71. Waterhouse BD, Chandler DJ. Heterogeneous organization and function of the central noradrenergic system. Brain Res 2016; 1641(Pt B): v–x. [PubMed: 26746339]

72. Gomez JL, Bonaventura J, Lesniak W, Mathews WB, Sysa-Shah P, Rodriguez LA et al. Chemogenetics revealed: DREADD occupancy and activation via converted clozapine. Science 2017; 357(6350): 503–507. [PubMed: 28774929]

73. Manvich DF, Webster KA, Foster SL, Farrell MS, Ritchie JC, Porter JH et al. The DREADD agonist clozapine N-oxide (CNO) is reverse-metabolized to clozapine and produces clozapine-like interoceptive stimulus effects in rats and mice. Sci Rep 2018; 8(1): 3840. [PubMed: 29497149]

74. Hyttel J Effects of a single administration of clozapine on mouse brain catecholamines. Acta Pharmacol Toxicol (Copenh.) 1976; 38(4): 358–365. [PubMed: 946734]

75. Robertson SD, Matthies HJ, Owens WA, Sathananthan V, Christianson NS, Kennedy JP et al. Insulin reveals Akt signaling as a novel regulator of norepinephrine transporter trafficking and norepinephrine homeostasis. J Neurosci 2010; 30(34): 11305–11316. [PubMed: 20739551]

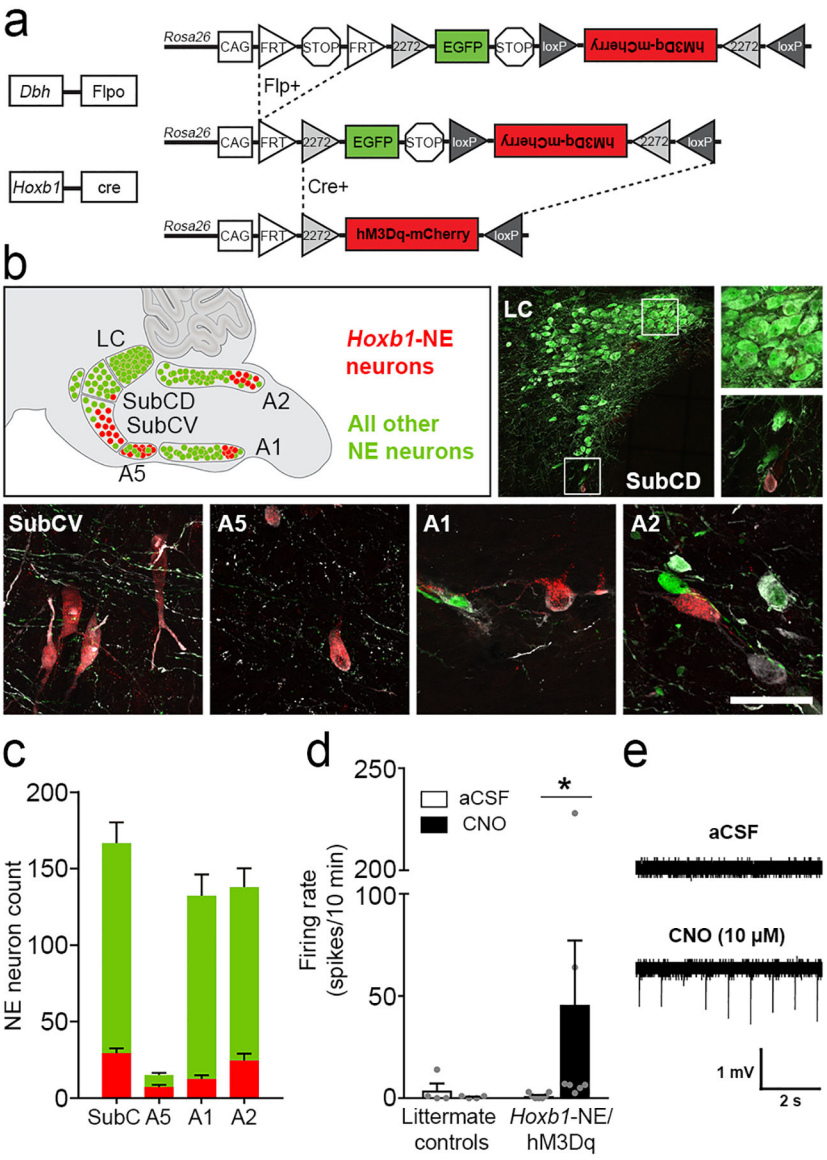

Figure 1. Intersectional chemogenetic strategy to selectively activate *Hoxb1*-NE neurons.

(**a**) Schematic diagram of the *RC::FL-hM3Dq* allele. Recombination by Dbh^{Flpo} leads to EGFP expression in NE neurons, and recombination by both $Hoxb1^{Cre}$ and Dbh^{Flpo} leads to hM3Dq-mCherry expression in *Hoxb1*-NE neurons. (**b**) Approximate positions of noradrenergic nuclei are illustrated on a sagittal schematic diagram of the hindbrain compressed along the mediolateral axis. Immunofluorescent labeling of parasagittal sections from *Hoxb1*-NE/hM3Dq brains for tyrosine hydroxylase (white), mCherry (red) and EGFP (green) reveals hM3Dq-mCherry-expressing *Hoxb1*-NE neurons in dorsal and ventral subcoeruleus (SubCD and SubCV), A5, caudal A1, and caudal A2 noradrenergic nuclei, but not in the locus coeruleus. Scale bar: 287 μm (LC), 100 μm (LC and SubCD close-ups), 50 μm (SubCV, A5, A1, A2). (**c**) Counts of hM3Dq-mCherry-expressing (red bars) and EGFP-expressing NE neurons (green bars) in different nuclei (n=12 mice). (**d**) Bath application of CNO (10 μM) increases firing rate in hM3Dq-mCherry-expressing neurons (*Hoxb1*-NE/

hM3Dq mice, n=7 cells from 5 mice), but not in EGFP-expressing neurons (littermate control mice, n=4 cells from 2 mice). Data are mean ± SEM. *P<0.05 vs. aCSF, Wilcoxon signed ranks test. (**e**) Representative traces of cell-attached recordings from hM3Dq-mCherry-expressing neurons before (top) and after (bottom) bath application of CNO (10 μM).

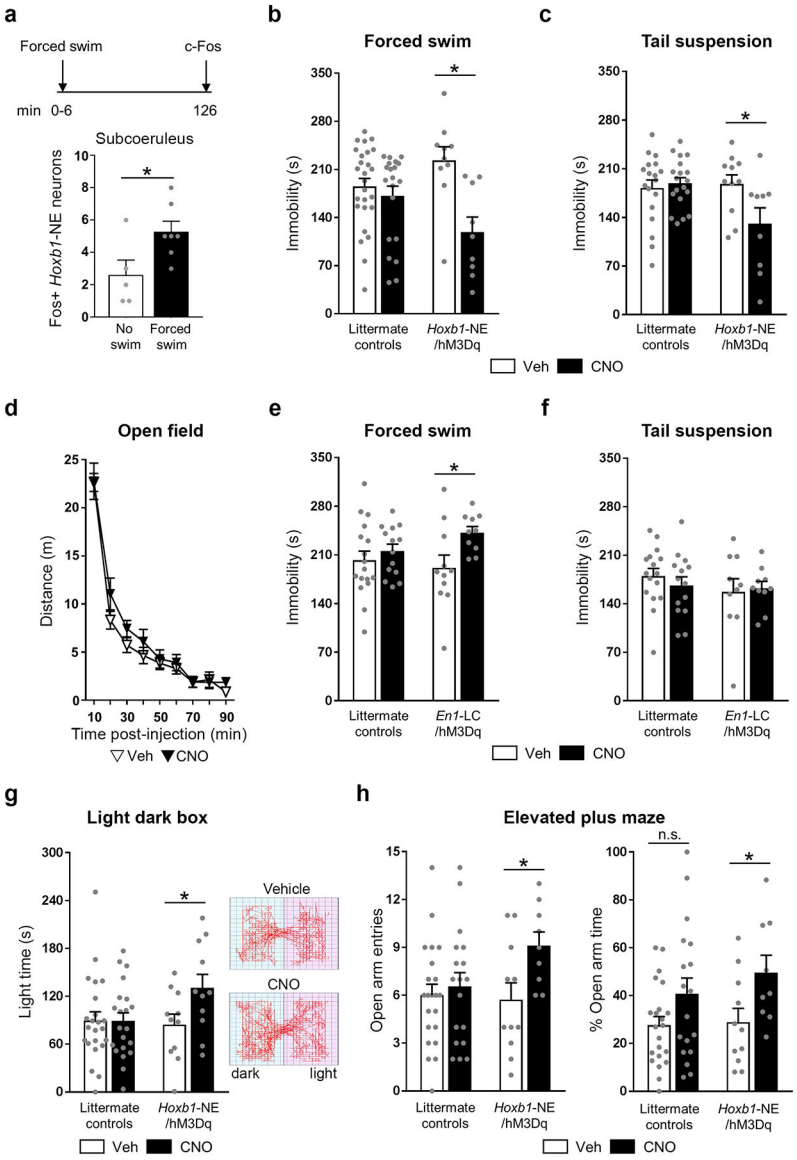

Figure 2. Chemogenetic activation of *Hoxb1*-NE neurons attenuates behavioral stress responses.

(**a**) Top: time line of the experiment. Bottom: Fos immunohistochemistry shows that subcoeruleus *Hoxb1*-NE neurons are activated by forced swim stress (no swim: n=5; forced swim: n=7). (**b-c**) Activation of *Hoxb1*-NE neurons reduces immobility time in the forced swim (littermate controls vehicle: n=26; littermate controls CNO: n= 21; *Hoxb1*-NE/hM3Dq vehicle: n=10; *Hoxb1*-NE/hM3Dq CNO: n=9) and tail suspension (littermate controls vehicle: n=18; littermate controls CNO: n=19; *Hoxb1*-NE/hM3Dq vehicle: n=11; *Hoxb1*-NE/hM3Dq CNO: n=9) tests. (**d**) Activation of *Hoxb1*-NE neurons does not affect locomotion in the open field (*Hoxb1*-NE/hM3Dq vehicle: n=11; *Hoxb1*-NE/hM3Dq CNO: n=11). (**e-f**) Activation of LC-NE increases immobility time in the forced swim test (littermate controls vehicle: n=17; littermate controls CNO: n=14; *En1*-LC/hM3Dq vehicle: n=11; *En1*-LC/hM3Dq CNO: n=10) but does not affect performance in the tail suspension test (littermate controls vehicle: n=16; littermate controls CNO: n=14; *En1*-LC/hM3Dq

vehicle: n=10; *En1*-LC/hM3Dq CNO: n=10). (**g**) Left: Activation of *Hoxb1*-NE neurons increases time exploring the light compartment of the light dark box (littermate controls vehicle: n=23; littermate controls CNO: n=21; *Hoxb1*-NE/hM3Dq vehicle: n=11; *Hoxb1*-NE/hM3Dq CNO: n=11). Right: Representative traces from vehicle- (top) and CNO-treated (bottom) *Hoxb1*-NE/hM3Dq mice. (**h**) Activation of *Hoxb1*-NE neurons increases number of entering (left) and % time exploring (right) the open arm of the elevated plus maze (littermate controls vehicle: n=22; littermate controls CNO: n=18; *Hoxb1*-NE/hM3Dq vehicle: n=11; *Hoxb1*-NE/hM3Dq CNO: n=9). Data are mean ± SEM. *P<0.05 vs. no swim (unpaired 2-tailed *t*-test) or Vehicle (*a priori* unpaired *t*-test for light dark box and unpaired 2-tailed *t*-test following two-way ANOVA for all other tests).

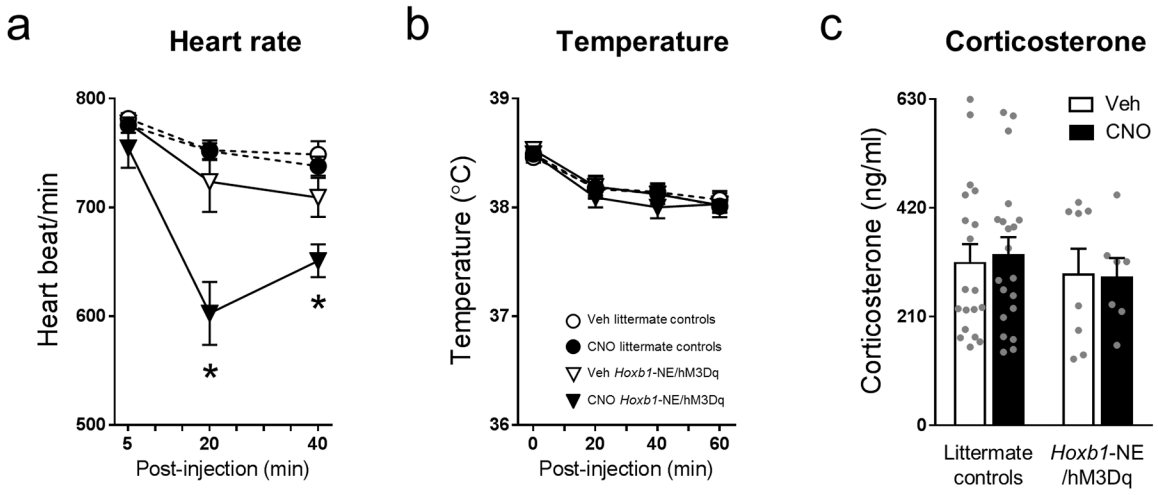

Figure 3. Chemogenetic activation of *Hoxb1*-NE neurons reduced heart rate with no effect on body temperature or corticosterone level.

Physiological measurement data from (**a**) heart rate (littermate controls vehicle: n=16; littermate controls CNO: n=17; *Hoxb1*-NE/hM3Dq vehicle: n=6; *Hoxb1*-NE/hM3Dq CNO: n=6), (**b**) body temperature (littermate controls vehicle: n=29; littermate controls CNO: n= 29; *Hoxb1*-NE/hM3Dq vehicle: n=12; *Hoxb1*-NE/hM3Dq CNO: n=12), and (**c**) serum corticosterone level (littermate controls vehicle: n=19; littermate controls CNO: n= 20; *Hoxb1*-NE/hM3Dq vehicle: n=8; *Hoxb1*-NE/hM3Dq CNO: n=7). Data are mean ± SEM, *P<0.05 vs. Vehicle (unpaired 2-tailed *t*-test at specific time points following repeated measures ANOVA).

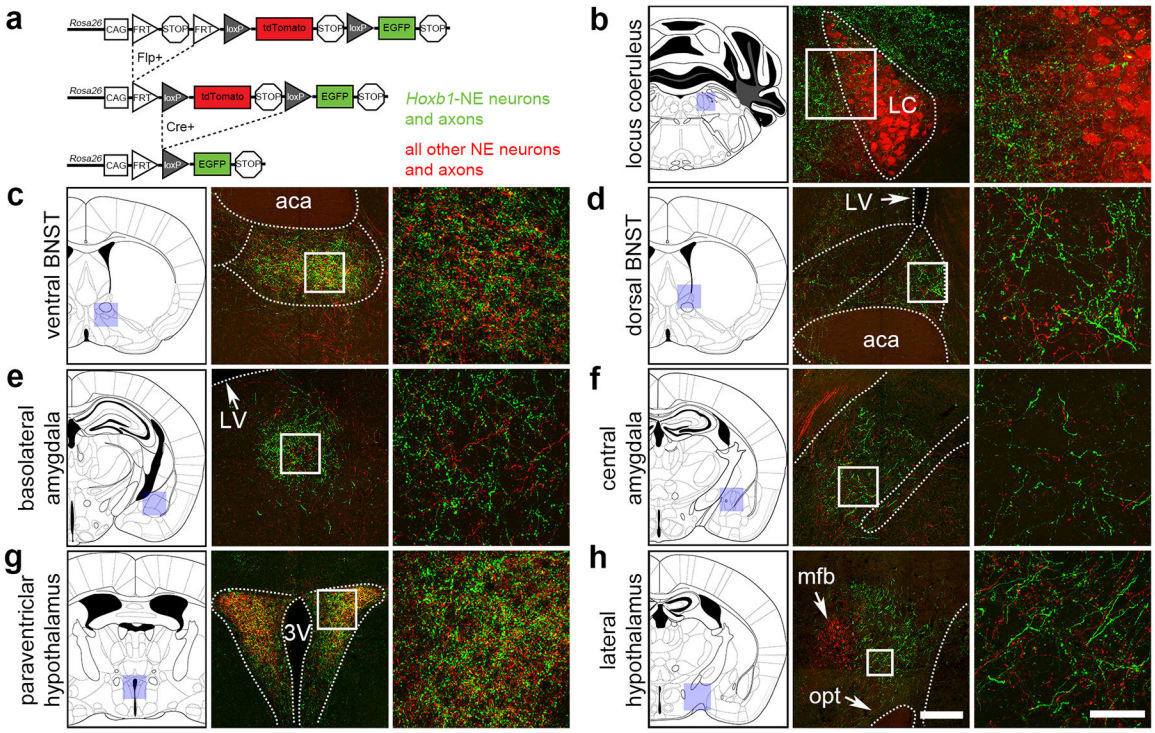

Figure 4. *Hoxb1*-NE axons are intermingled with axons of other NE neurons at stress-related brain regions.

(**a**) Schematic diagram of a dual Flp/Cre-responsive fluorescent indicator allele *RC::FLTG*. Recombination by Dbh^{Flpo} leads to tdTomato expression in NE neurons and axons, and recombination by both $Hoxb1^{Cre}$ and Dbh^{Flpo} leads to EGFP expression in *Hoxb1*-NE neurons and axons. (**b-h**) In mice heterozygous for $Hoxb1^{Cre}$, Dbh^{Flpo}, and *RC::FLTG*, *Hoxb1*-NE axons (EGFP+) are intermingled with axons arising from other NE neurons (tdTomato+, including LC neurons). Shaded boxes on the coronal schematic diagrams indicate the approximate position of the low magnification images, and white boxes indicate position of the high magnification images. Dotted lines indicate approximate boundaries of anatomical regions. aca, anterior commissure; 3V, third ventricle; LV, lateral ventricle; mfb, medial forebrain bundle; opt, optic tract. Scale bar for low-mag. images: 200 μm (100 μm LC, 300 μm lateral hypothalamus). Scale bar for high-mag. images: 50 μm.

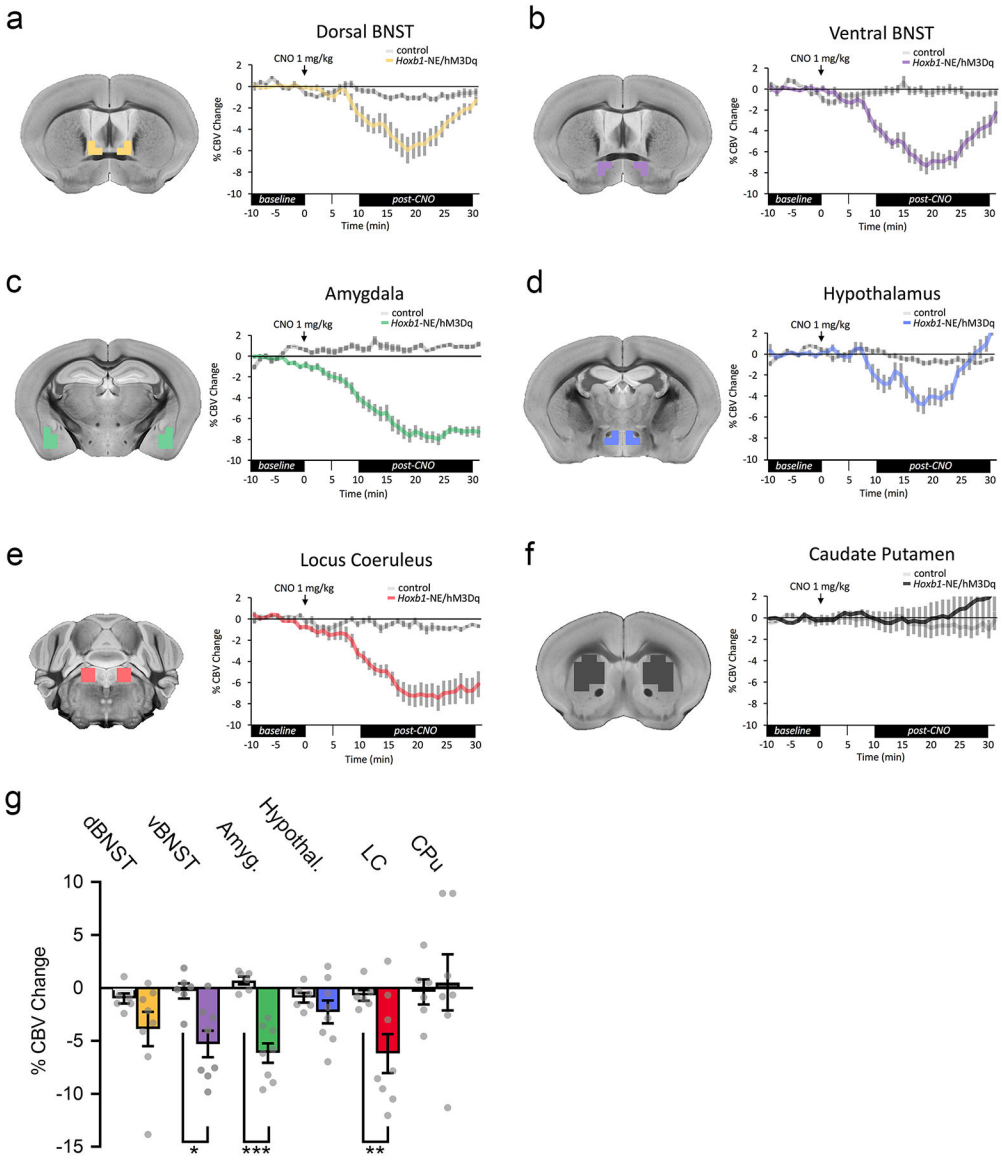

Figure 5. Chemogenetic activation of *Hoxb1*-NE neurons results in significant decrease in CBV at stress-related targets.

(**a-f**) CBV-weighted fMRI traces from the color-coded regions of interest depicted in representative coronal scans show decreased CBV in dorsal BNST (*yellow*), ventral BNST (*purple*), amygdala (*green*), hypothalamus (*blue*), and locus coeruleus (*red*) but no change in the caudate putamen (black) of *Hoxb1*-NE/hM3Dq mice following 1 mg/kg CNO administration (n=7–8). No change was observed in the controls (n=6). Error bars represent ± SEM. (**g**) Bar graph shows comparison of CBV-weighted fMRI signal changes between baseline (first 10 min) and post-CNO (final 20 min) in control and *Hoxb1*-NE/hM3Dq mice. *P< 0.05, **P<0.01, ***P<0.001, unpaired 2-tailed *t*-test. Data are displayed as mean ± SEM.